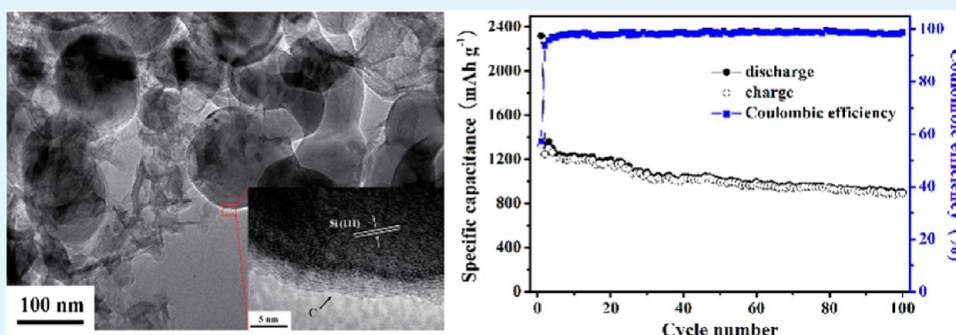


# Graphene/Carbon-Coated Si Nanoparticle Hybrids as High-Performance Anode Materials for Li-Ion Batteries

Min Zhou, Tingwei Cai, Fan Pu, Hao Chen, Zhao Wang, Haiyong Zhang, and Shiyong Guan\*

School of Materials Science and Engineering, East China University of Science and Technology, Mei Long Road 130, Shanghai 200237, P.R. China



**ABSTRACT:** Si is regarded as one of the most promising anode materials for next generation Li-ion batteries, but it usually exhibits poor cycling stability due to the low intrinsic electrical conductivity and huge volume change induced by the alloying reaction with Li. In this study, we present a double protection strategy by fabricating graphene/carbon-coated Si nanoparticle hybrids to improve the electrochemical performance of Si in Li storage. The Si nanoparticles are wrapped between the graphene and the amorphous carbon coating layers in the hybrids. The graphene and the amorphous carbon coating layers work together to effectively suppress the aggregation and destruction of Si nanoparticles, keeping the overall electrode highly conductive and active in Li storage. As a result, the produced graphene/carbon-coated Si nanoparticle hybrids exhibit outstanding reversible capacity for Li storage (902 mAh g<sup>-1</sup> after 100 cycles at 300 mA g<sup>-1</sup>). This work suggests a strategy to improve the electrochemical performance of Li-ion batteries by using graphene as supporting sheets for loading of active materials and carbon as the covering layers.

**KEYWORDS:** Si, carbon, graphene, anode materials, Li-ion batteries, cycling stability, capacity

## 1. INTRODUCTION

The development of high energy density and long cycle life Li-ion batteries is of great interest for use in portable electronics, electric vehicles, and the storage of renewable energy.<sup>1–3</sup> To meet these requirements, the electrode materials of Li-ion batteries must have high specific storage capacities and satisfactory cycle life. Alloy-type anodes (Si, Ge, Sn, Al, Sb, etc.) have much higher Li storage capacity than the intercalation-type graphite anode that is currently used in Li-ion batteries.<sup>4</sup> Among all the alloy anodes, Si has the highest theoretical specific capacity of 4200 mAh g<sup>-1</sup>, which is 10 times higher than that of graphite (372 mAh g<sup>-1</sup>).<sup>5–7</sup> The practical application of Si as an anode material is, however, seriously hindered by the significant volume changes (>300%, which leads to dramatic destruction of the initial particle morphology and the loss of electrical contact between active materials and the electrode framework) and low intrinsic electrical conductivity during Li insertion/extraction from Si, resulting in rapid capacity fading.<sup>8–10</sup>

Tremendous efforts have been made to overcome these issues and improve the overall electrochemical performance of Si anodes. One effective strategy is to reduce the size of bulk Si

to the sub-micrometer scale in at least one dimension, such as nanowires and nanotubes, which can effectively avoid fracture and therefore improve the cycling performance.<sup>11,12</sup> However, nanowires and nanotubes, which are expensive and difficult to scale up, suffer from limited overall charge storage capacity due to a low mass fraction of the active component in the electrode.<sup>13</sup> Fabricating porous electrode frameworks using sacrificial templates is another approach.<sup>14,15</sup> However, these porous electrodes introduce different problems, such as configurational inflexibility imposed by mechanical fragility and a dramatic drop in volumetric energy density consequential of reduced packing densities.<sup>13</sup> Dispersing Si into a carbon matrix has been well developed in which the carbonaceous materials can buffer the volume change and improve the electrical conductivity of Si active materials.<sup>16–22</sup> Different kinds of carbon materials including amorphous carbon,<sup>16,17</sup> graphite,<sup>18</sup> carbon nanotubes,<sup>19,20</sup> carbon nanofibers,<sup>21,22</sup> etc.,

Received: February 7, 2013

Accepted: March 25, 2013

Published: March 25, 2013

have been investigated to improve the cycling stability of Si active materials.

Graphene, a two-dimensional carbon nanomaterial, has attracted enormous attention owing to its unique properties and potential applications in the areas of electronics as well as energy conversion and storage devices.<sup>23–26</sup> Recent work has shown that graphene can greatly improve the reversible capacity, cycling stability, and rate capability of Li-ion batteries' electrodes as a conducting and buffering matrix.<sup>27–30</sup> However, in the cases of Si-based anode materials, there are still many difficulties in the utilization of graphene.<sup>13,31–37</sup> For example, the exposed Si nanoparticles on the graphene surface are still prone to aggregate and disintegrate. Meanwhile, the volume expansion rates of Si nanoparticles and graphene are significantly different, which may result in Si nanoparticles peeling off from the graphene after several charge/discharge cycles. These handicaps can lead to a decreased electrochemical performance of graphene–Si (G–Si) hybrids.

Recently, Luo et al. prepared sub-micrometer-sized capsules made of Si nanoparticles wrapped by crumpled graphene shells by a rapid, one-step capillary-driven assembly route in aerosol droplets.<sup>38</sup> The folds and wrinkles in the crumpled graphene coating can accommodate the volume expansion of Si upon lithiation without fracture, and the composite capsules have greatly improved performance as Li-ion battery anodes in terms of capacity, cycling stability, and Coulombic efficiency. Here, we report another approach to greatly improve the electrochemical performance of G–Si hybrids by further coating a thin layer of amorphous carbon on the Si nanoparticles after the Si nanoparticles are well dispersed on the graphene surface. In this way, Si nanoparticles are properly wrapped between graphene and the amorphous carbon coating layers. The graphene and the amorphous carbon coating layers work together to effectively maintain the stability of the structural arrangement, suppress the aggregation and destruction of Si nanoparticles, and serve as good electron conductors. The complete fabrication of graphene/carbon-coated Si nanoparticle (G–Si–C) hybrids includes two steps: dispersing Si nanoparticles on the graphene surface and then coating a thin layer of amorphous carbon on the Si nanoparticles.

It is known that Si nanoparticles are easy to oxidize to form a layer of silicon oxide on its surface; thus, they can be easily modified by surface grafting of aminopropyltriethoxysilane (APS) to render the surface chemically positive charged in acid solution due to ionization of amino groups of APS.<sup>39,40</sup> Graphene oxide (GO) shows a negative charge over the pH range (2–11) owing to ionization of the carboxylic acid and phenolic hydroxyl groups existing on the GO.<sup>41,42</sup> Therefore, the Si nanoparticles can be well dispersed on the graphene surface by hybrid electrostatic assembly between APS modified Si nanoparticles (Si-APS) and GO, and followed by thermal reduction.

Recently, the specific ionic liquids are used as new precursors to obtain carbon materials.<sup>43–47</sup> Compared with conventional solid carbon precursors, the specific ionic liquids can penetrate into nanospaces easily, owing to their fluidic properties. The specific ionic liquids can be pyrolyzed in inert atmosphere without evaporation, which is favorable for forming a thin uniform coating layer. Here, a specific ionic liquid (1-ethyl-3-methylimidazolium dicyanamide<sup>43,47,48</sup>) is chosen as the carbon precursor to form a thin layer of amorphous carbon on the Si nanoparticles.

As a result, the as-prepared G–Si–C hybrids exhibit superior electrochemical performance with large reversible capacity and excellent cycling performance when used as anode materials for Li-ion batteries.

## 2. EXPERIMENTAL SECTION

**2.1. Sample Preparation.** Graphite oxide was first synthesized by a modified Hummers method.<sup>49</sup> GO was exfoliated from the graphite oxide through an ultrasonication process.<sup>50</sup> The G–Si hybrids were prepared through hybrid electrostatic assembly between Si-APS and GO, followed by thermal reduction.<sup>41</sup> The ionic liquid 1-ethyl-3-methylimidazolium dicyanamide was chosen as the carbon precursor to form a thin layer of amorphous carbon on the Si nanoparticles, for it had been demonstrated to obtain nitrogen-doped carbon after pyrolysis in inert atmosphere<sup>43,47,48</sup> and the nitrogen-doped carbon probably benefited the electrochemical performance, since nitrogen doping had been reported to facilitate the electronic conductivity of the carbon layers and the charge transfer at the interface.<sup>48</sup> In a typical experiment, 500 mg of Si nanoparticles (<200 nm) were dispersed into 50 mL of dry toluene solution via sonication for 1 h and then 0.5 mL APS was poured into and stirred at 40 °C for 24 h under a nitrogen atmosphere to obtain Si-APS. 400 mL of Si-APS suspension (0.5 mg mL<sup>-1</sup>) containing 0.4 mL of HCl (36 wt %) was added slowly into 1000 mL of GO suspension (0.08 mg mL<sup>-1</sup>) under mild magnetic stirring at 40 °C. After 24 h, the product was separated, dried, and reduced at 800 °C for 3 h under nitrogen to obtain the G–Si hybrids. To coat a thin layer of amorphous carbon on the Si nanoparticles, 200 mg of G–Si hybrids was added to 0.7 mL of the ionic liquid 1-ethyl-3-methylimidazolium dicyanamide. After magnetic stirring for 12 h at room temperature, the obtained product was pyrolyzed at 600 °C for 1 h under nitrogen to obtain the G–Si–C hybrids.

**2.2. Sample Characterization.** Powder X-ray diffraction (XRD) patterns were obtained on a D/MAX 2550VB/PC diffractometer (Rigaku, Japan) using Cu K $\alpha$  radiation ( $\lambda = 0.154$  nm). Raman spectra were recorded using an InVia Raman microscope (Renishaw, UK) with 514.5 nm diode laser excitation. Thermogravimetric analysis (TGA) was performed on a STA409PC analyzer (Netzsch, Germany) under air with a ramp rate of 10 °C min<sup>-1</sup>. Field emission scanning electron microscopy (FE-SEM) measurement was conducted on a S-4800 (Hitachi, Japan) instrument. Transmission electron microscopy (TEM) images were collected on a JEM-2100 (JEOL, Japan) instrument.

**2.3. Electrochemical Measurements.** The working electrodes were prepared by mixing 70 wt % active materials with 20 wt % carbon black and 10 wt % polyvinylidene difluoride binder in *N*-methyl-2-pyrrolidinone to form a homogeneous slurry, which was uniformly pasted onto copper foil. The prepared working electrodes were dried in a vacuum oven at 100 °C over 12 h and were then ready for assembly in test cells. Electrochemical cells (CR2016 coin type) using the active materials as the working electrode, Li foil as the counter electrode and reference electrode, a microporous polypropylene film as the separator, and 1 M LiPF<sub>6</sub> in ethylene carbonate/dimethyl carbonate (1:1 by volume) with 2 wt % vinylene carbonate as the electrolyte were assembled in an Ar-filled glovebox. The cells were galvanostatically charged and discharged over a voltage range of 0.02–1.2 V versus Li/Li<sup>+</sup> at a current density of 300 mA g<sup>-1</sup>. The specific capacity values were calculated on the basis of the total weight of active materials. The electrochemical impedance measurements were performed at an AC voltage of 5 mV amplitude in the 100 kHz to 0.01 Hz range.

## 3. RESULTS AND DISCUSSION

**3.1. Structure and Morphology.** Figure 1 shows the XRD patterns of the as-prepared samples, together with the XRD pattern of the pristine Si nanoparticles. The diffraction patterns of the G–Si hybrids and the G–Si–C hybrids are identical with that of the Si nanoparticles, indicating that the Si nanoparticles in the G–Si hybrids and the G–Si–C hybrids are still retained

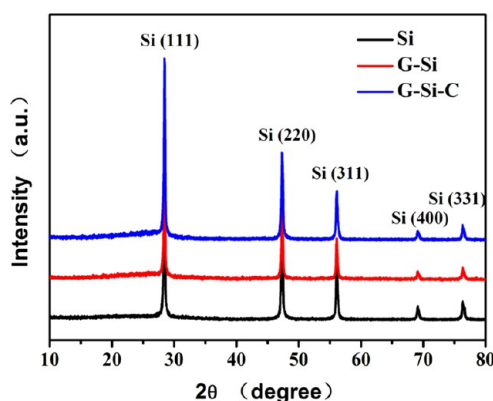


Figure 1. XRD patterns of Si, G-Si, and G-Si-C.

in the crystalline structure. It is difficult to clearly identify the graphene peaks and the crystalline carbon peaks in the XRD patterns. This may be due to the following factors: (1) the amorphous graphene is homogeneously distributed in the hybrids without stacking or agglomeration; (2) the carbon coating layers on the Si nanoparticles using the specific ionic liquid as the precursor are amorphous, and the intensity of amorphous carbon peaks is much lower in comparison with those of crystalline Si peaks; (3) both the amounts of graphene and amorphous carbon are low.

Figure 2 presents the Raman spectra of the G-Si hybrids and the G-Si-C hybrids, with the Raman spectrum of the Si

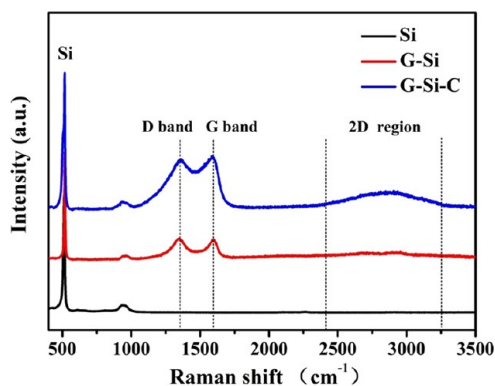


Figure 2. Raman spectra of Si, G-Si, and G-Si-C.

nanoparticles shown for comparison. For the G-Si hybrids and the G-Si-C hybrids, a main peak at about  $517\text{ cm}^{-1}$  is in agreement with the data in the spectrum of Si nanoparticles, while the peaks at  $1350$  and  $1596\text{ cm}^{-1}$  correspond to the D band and the G band, respectively, and the modulated bump at  $2400\text{--}3250\text{ cm}^{-1}$  is represented as the 2D region, which are all the characteristic Raman peaks for carbon materials.<sup>51–53</sup> However, the 2D region is not obvious in the spectrum of the G-Si hybrids, which may be due to the low amount of graphene and the nature of the 2D region, which is highly broadened and low intense.<sup>52</sup> The intensity ratio of D and G bands,  $I_D/I_G$ , of the G-Si hybrids is much smaller than that of GO (which is not shown here), indicating the successful reduction of GO to graphene. However, the intensity of the D band is still comparable to that of the G band. This may be due to a decrease in the average size of the new or more  $sp^2$  domains during the reduction.<sup>53</sup> It is clear that all the intensities of the D band, G band, and 2D region of the G-Si-C hybrids

are higher than those of the G-Si hybrids, indicating that the Si nanoparticles are coated with additional amorphous carbon after they are well dispersed on the graphene surface.

The thermal properties and the compositions of the samples were characterized by TGA in air. As shown in Figure 3, an

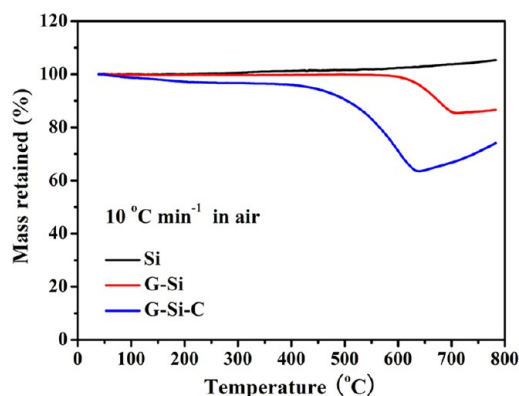


Figure 3. TGA curves of Si, G-Si, and G-Si-C.

abrupt weight loss occurs between  $600$  and  $700\text{ °C}$  for the G-Si hybrids, indicating the oxidation and decomposition of graphene in air. Here the graphene starts to get oxidized at about  $600\text{ °C}$ , which is higher than the temperatures reported in the literature.<sup>31,34</sup> We suppose that it may be due to the occurrence of interactions between the graphene sheets and Si nanoparticles. However, for the G-Si-C hybrids, the abrupt weight loss occurs at an onset reaction temperature of about  $400\text{ °C}$ , and the oxidation reaction with oxygen in air is completed at about  $640\text{ °C}$ . This may be due to the amorphous carbon coating layers on the Si nanoparticles and the difference of the oxidation and decomposition between the amorphous carbon and the graphene in air. Since the oxidation of Si nanoparticles in air is not significant, the change in weight before and after the oxidation of graphene or amorphous carbon can be translated into the amount of graphene or amorphous carbon in the samples, respectively. From the TGA curves, the mass fraction of graphene in the G-Si hybrids is about  $14.6\text{ wt } \%$ , and the total amount of graphene and carbon in the G-Si-C hybrids is about  $36.1\text{ wt } \%$ . Considering that the G-Si-C hybrids are prepared by further coating a layer of amorphous carbon on the Si nanoparticles after the Si nanoparticles are well dispersed on the graphene surface, and thus the mass ratio of Si to graphene is  $85.4:14.6$  in the G-Si-C hybrids, the amounts of graphene and amorphous carbon in the G-Si-C hybrids are around  $10.9$  and  $25.2\text{ wt } \%$ , respectively.

FE-SEM images (Figure 4a,b) show that the G-Si hybrids and the G-Si-C hybrids are micrometer-sized aggregates. Figure 4c shows the magnified FE-SEM image of the G-Si hybrids, in which both the wrinkles and edges (indicated with arrows) of the graphene and the Si nanoparticles are clearly observed. The presence of wrinkles and folds is the characteristic feature of graphene sheets. From Figure 4c, it can be clearly observed that the uniform distribution of the Si nanoparticles and the graphene is achieved in the G-Si hybrids through hybrid electrostatic assembly followed by thermal reduction. Figure 4d shows the magnified FE-SEM image of the G-Si-C hybrids, in which much less Si nanoparticles can be observed in comparison with that of the G-Si hybrids and the graphene is also not obvious. This may

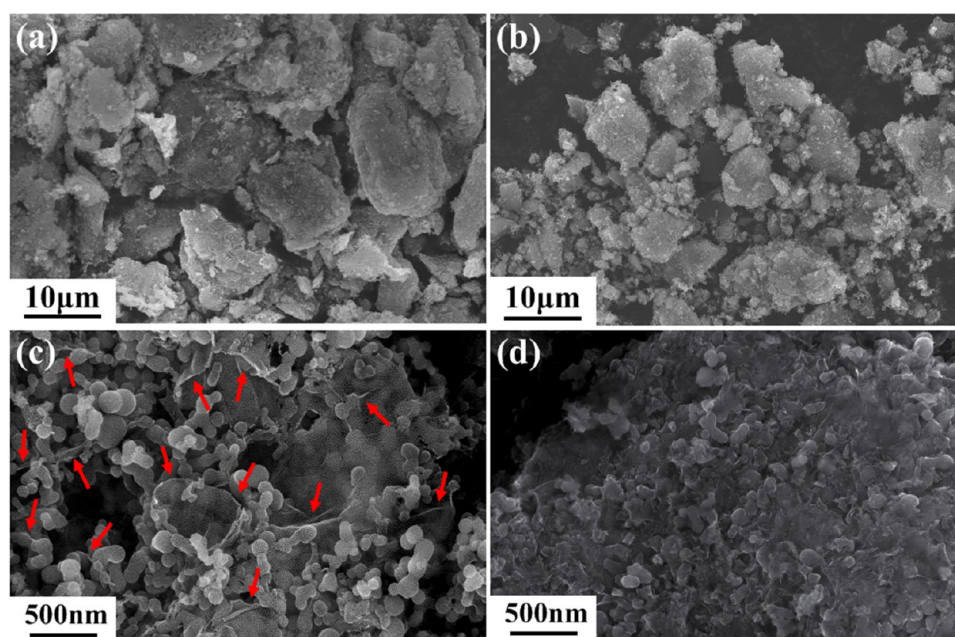


Figure 4. FE-SEM images of (a, c) G-Si and (b, d) G-Si-C.

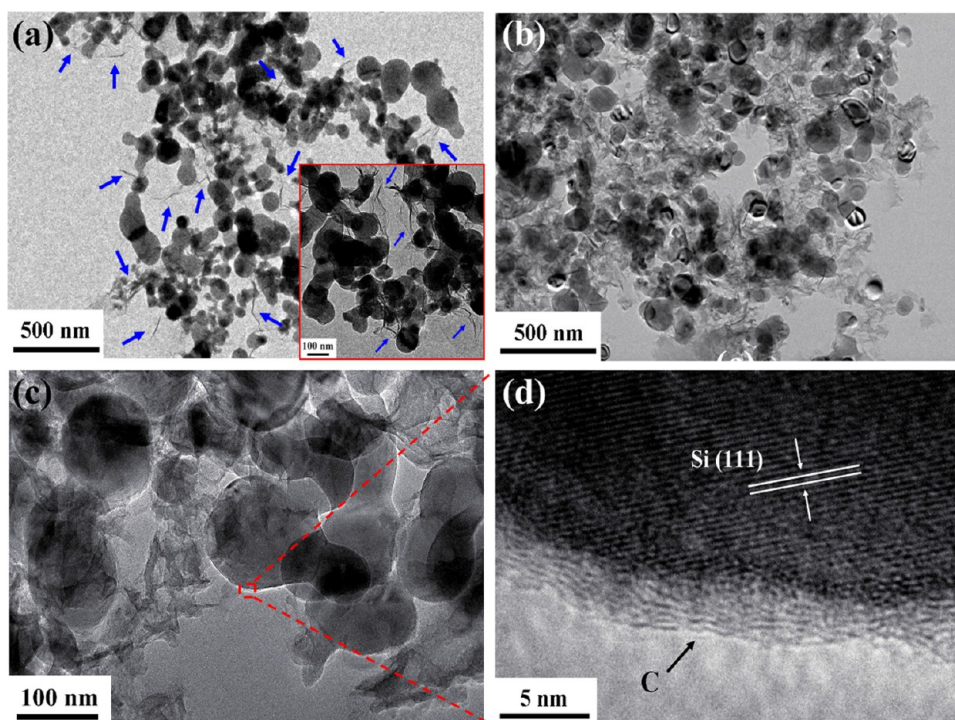
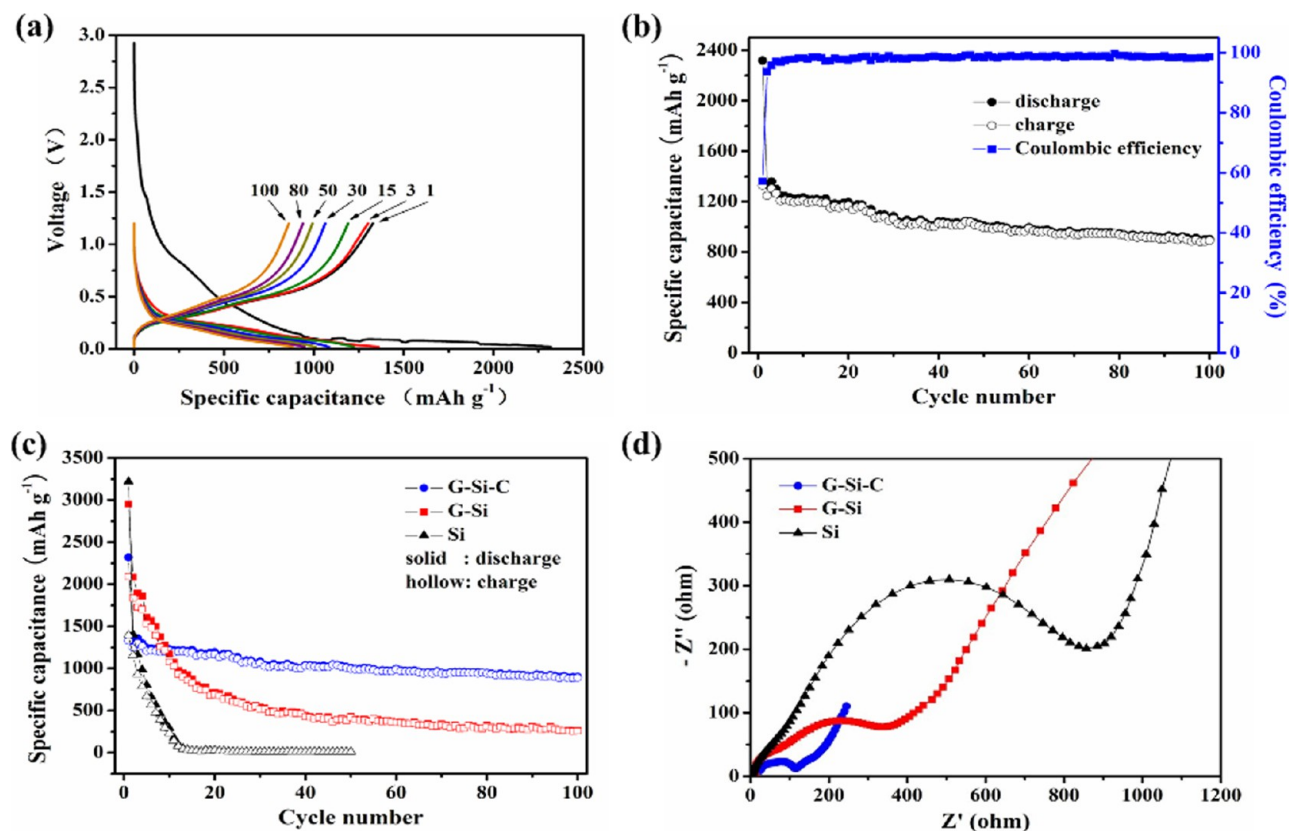


Figure 5. TEM images of (a) G-Si and (b–d) G-Si-C. The inset of part a is a magnified TEM image of G-Si.

be due to additional carbon layers coating on the Si nanoparticles and filling the nanospaces existing between the Si nanoparticles and the graphene.

Figure 5 shows the TEM images of the G-Si hybrids and the G-Si-C hybrids. Due to the ultrathin structure and the low contrast of graphene, only the wrinkles and folds (indicated by arrows), which are the characteristic features of the graphene sheets, can be observed in the G-Si hybrids (Figure 5a). The inset of Figure 5a shows a magnified TEM image of the G-Si hybrids, in which the graphene sheets can be clearly observed, especially the folds and edges (indicated by arrows) of the

graphene sheets. Apparently, the Si nanoparticles are spread over the graphene surface, and firmly attached to graphene sheets even after an ultrasonic process, which was used to prepare the samples for TEM characterization, indicating the strong interactions between Si nanoparticles and graphene sheets. It is worth noting that not any unattached Si nanoparticles or graphene sheets can be found in the TEM visualizations. Also not any obvious aggregation of Si nanoparticles on the graphene surface can be found, indicating the uniform distribution of Si nanoparticles and graphene in the G-Si hybrids. Figure 5b–d shows the TEM images of the G-



**Figure 6.** (a) Voltage profiles of G-Si-C; (b) cycling performance and Coulombic efficiency of G-Si-C; (c) cycling performance of Si, G-Si, and G-Si-C; and (d) Nyquist plots of Si, G-Si, and G-Si-C.

Si-C hybrids. Many crinkled sheets with morphology similar to but contrast higher than that of graphene can be observed (Figure 5b,c). These crinkled sheets are the graphene covered by some amorphous carbon nanoparticles, in which the sizes of the amorphous carbon nanoparticles are much smaller than those of graphene in the plane range. Notably, the HR-TEM image (Figure 5d) shows that the Si nanoparticle is coated with a thin uniform layer of amorphous carbon (2–3 nm in thickness). Therefore, the Si nanoparticles are wrapped between the graphene and the amorphous carbon coating layers.

In short, the above results suggest that the G-Si-C hybrids are composed of Si nanoparticles, graphene, and amorphous carbon, the Si nanoparticles are well dispersed on the graphene surface, and a thin uniform amorphous carbon layer is coated on the Si nanoparticles. The unique structure is expected for superior Li storage, because the graphene and the amorphous carbon coating layers can work together to provide a perfect conductive carbon network for facilitating electron transfer, buffering the volume changes, preventing aggregation and destruction of Si nanoparticles, and maintaining the structure stable during the Li insertion/extraction.

**3.2. Electrochemical Performance.** Figure 6a shows the typical charge–discharge curves of the cells with the G-Si-C hybrids as anodes for Li-ion batteries at a current density of 300 mA g<sup>-1</sup> between 0.02 and 1.2 V vs Li/Li<sup>+</sup>. In the first discharging (alloying reaction between Si and Li) curve, two main plateaus appear at ~0.8 and ~0.1 V. The absence of the former plateau in the following cycles strongly indicates that this is associated with electrolyte decomposition and concomitant solid electrolyte interface (SEI) formation on

the electrode surface.<sup>54</sup> The long flat plateau at ~0.1 V is indicative of the alloying reaction between crystalline Si and Li.<sup>55</sup>

The variation of specific gravimetric capacity with cycle number of the G-Si-C anode is shown in Figure 6b. The first discharge and charge capacities are 2319 and 1328 mAh g<sup>-1</sup>, respectively (the capacity values are calculated on the basis of the G-Si-C hybrid mass), with an initial Coulombic efficiency of 57.3%, corresponding to an irreversible capacity loss of 42.7%. The lower initial Coulombic efficiency is caused by the formation of the solid electrolyte interphase (mentioned above), which may be due to the high surface area of the graphene. It has been reported that graphene anodes show large irreversible capacity in the first cycle, which is associated with the formation of a SEI layer.<sup>56,57</sup> However, the Coulombic efficiency soon reaches nearly 100% and remains relatively stable in subsequent cycles. It is striking to note that a discharge capacity of 902 mAh g<sup>-1</sup> is retained after 100 cycles. This value is much higher than the theoretical specific capacity of the graphite electrode (372 mAh g<sup>-1</sup>). These indicate that a stable SEI film is formed and a stable electrical contact of the active Si is maintained during cycling despite the drastic dimensional change.

For comparison, the electrochemical performance of the G-Si hybrids and the pristine Si nanoparticles was also investigated under the same electrochemical condition. As illustrated in Figure 6c, the G-Si-C hybrids show much better cycle performance than the G-Si hybrids and the pristine Si nanoparticles. The Si nanoparticles exhibit a initial discharge capacity of 3220 mAh g<sup>-1</sup>; however, the capacity drops dramatically to 13 mAh g<sup>-1</sup> after only 50 cycles. This would be

attributed to the poor intrinsic electronic conductivity and the dramatic destruction of the initial particle morphology of Si nanoparticles during Li insertion/extraction, leading to the loss of electrical contact between active materials and the electrode framework. Moreover, although the weight content of Si in the G–Si hybrids (~85 wt %) is higher than that in the G–Si–C hybrids (~64 wt %), the specific capacity of the G–Si hybrids decreases gradually from 2949 mAh g<sup>-1</sup> at the first cycle to 263 mAh g<sup>-1</sup> after 100 cycles. This may be due to the exposed Si nanoparticles on the graphene surface aggregated and disintegrated or peeled off from the graphene after several charge/discharge cycles. These results demonstrate that the amorphous carbon coating layers on the Si nanoparticles play a crucially important role in the excellent cycle performance of the G–Si–C hybrids, for they can alleviate the effects of volume changes, stabilize the structure, and increase the conductivity. Even though the amorphous carbon coating layers would be disrupted after the Si expansion, we suppose that the disrupted amorphous carbon could still adhere to the surface of the Si nanoparticles, which can not only act as a barrier to suppress the aggregation of Si nanoparticles but also construct efficient conducting networks with the graphene for the Si nanoparticles.

To verify the good electrochemical performance of the G–Si–C hybrids in comparison with the G–Si hybrids and Si nanoparticles, AC impedance spectra measurements were carried out. Figure 6d shows AC impedance spectra of the sample electrodes after 100 cycles for G–Si–C hybrids and G–Si hybrids and 50 cycles for Si nanoparticles. A depressed semicircle in the high frequency range and an angled straight line in the low frequency range can be observed for all the cells. The diameter of the depressed semicircle mainly represents the charge transfer resistance, and the angled straight line is related to a diffusion controlled process.<sup>58</sup> Apparently, the diameter of the semicircle for the G–Si–C electrode is much smaller than those of the G–Si electrode and Si electrode, indicating that the G–Si–C electrode possesses the lowest resistance of the interfacial electrochemical reaction, which can be explained by the stable structure and the improved conductivity of the G–Si–C hybrids upon cycling.

It is well-known that the poor electrochemical performance of a Si negative electrode is due to the electrical isolation of the electrode in the cycling process arising from the semiconductor nature and destruction of Si active materials.<sup>8–10</sup> Therefore, the superior electrochemical performance of the G–Si–C hybrids for Li storage can be assigned to the synergistic effects of graphene, Si nanoparticles, and the amorphous carbon coating layers: (1) the combination of graphene and amorphous carbon coating layers gives rise to a high electrical conductivity of the overall electrode and thus increases electron transport rate; (2) the Si nanoparticles uniformly disperse on the graphene surface; (3) the flexible graphene and the elastic coated carbon layers can work together to accommodate the severe volume change and suppress the aggregation and destruction of Si nanoparticles upon Li insertion/extraction, thus improving the structural stability.

#### 4. CONCLUSION

In order to improve the electronic conduction and structural stability of a Si negative electrode for Li-ion batteries, we have developed a novel method for the preparation of graphene/carbon-coated Si nanoparticles hybrids. The G–Si–C hybrids are synthesized by further coating a thin layer of amorphous

carbon on the Si nanoparticles using ionic liquid as the carbon precursor after the Si nanoparticles are well dispersed on the graphene surface. When tested for Li storage, the as-achieved G–Si–C hybrids exhibit remarkably improved cycling performance in comparison with the G–Si hybrids and the bare Si nanoparticles. A high discharge capacity of 902 mAh g<sup>-1</sup> can be retained after 100 cycles at a current density of 300 mA g<sup>-1</sup>. This strategy, which employs graphene as supporting sheets for loading of active materials and carbon as the covering layers, is demonstrated to be an effective way to improve the cycling performance of anode materials for Li-ion batteries. It is supposed that further carbon coating with ionic liquids as carbon precursors pyrolyzed at moderate temperature, which is relatively simple, yet very effective, can be further extended to the fabrication of other materials with promising applications in catalysis, sensing, supercapacitors, and fuel cells.

#### AUTHOR INFORMATION

##### Corresponding Author

\*Phone/Fax: +86-21-64251509. E-mail: syguan@ecust.edu.cn.

##### Notes

The authors declare no competing financial interest.

#### ACKNOWLEDGMENTS

This research was financially supported by National Natural Science Foundation of China (No. 21274043).

#### REFERENCES

- (1) Armand, M.; Tarascon, J. M. *Nature* **2008**, *451*, 652–657.
- (2) Chen, J.; Cheng, F. Y. *Acc. Chem. Res.* **2009**, *42*, 713–723.
- (3) Goodenough, J. B.; Kim, Y. *Chem. Mater.* **2010**, *22*, 587–603.
- (4) Zhang, W.-J. *J. Power Sources* **2011**, *196*, 13–24.
- (5) Chan, C. K.; Peng, H.; Liu, G.; McIlwrath, K.; Zhang, X. F.; Huggins, R. A.; Cui, Y. *Nat. Nanotechnol.* **2008**, *3*, 31–35.
- (6) Magasinski, A.; Dixon, P.; Hertzberg, B.; Kvit, A.; Ayala, J.; Yushin, G. *Nat. Mater.* **2010**, *9*, 353–358.
- (7) Ma, H.; Cheng, F.; Chen, J.; Zhao, J.; Li, C.; Tao, Z.; Liang, J. *Adv. Mater.* **2007**, *19*, 4067–4070.
- (8) Oumellal, Y.; Delpuech, N.; Mazouzi, D.; Dupre, N.; Gaubicher, J.; Moreau, P.; Soudan, P.; Lestriez, B.; Guyomard, D. J. *J. Mater. Chem.* **2011**, *21*, 6201–6208.
- (9) Evanoff, K.; Magasinski, A.; Yang, J.; Yushin, G. *Adv. Energy Mater.* **2011**, *1*, 495–498.
- (10) Nguyen, H. T.; Yao, F.; Zamfir, M. R.; Biswas, C.; So, K. P.; Lee, Y. H.; Kim, S. M.; Cha, S. N.; Kim, J. M.; Pribat, D. *Adv. Energy Mater.* **2011**, *1*, 1154–1161.
- (11) Cui, L. F.; Ruffo, R.; Chan, C. K.; Peng, H.; Cui, Y. *Nano Lett.* **2009**, *9*, 491–495.
- (12) Park, M. H.; Kim, M. G.; Joo, J.; Kim, K.; Kim, J.; Ahn, S.; Cui, Y.; Cho, J. *Nano Lett.* **2009**, *9*, 3844–3847.
- (13) Zhao, X.; Hayner, C. M.; Kung, M. C.; Kung, H. H. *Adv. Energy Mater.* **2011**, *1*, 1079–1084.
- (14) Kim, H.; Cho, J. *Nano Lett.* **2008**, *8*, 3688–3691.
- (15) Zhang, H.; Yu, X.; Braun, P. V. *Nat. Nanotechnol.* **2011**, *6*, 277–281.
- (16) Datta, M. K.; Maranchi, J.; Chung, S. J.; Epur, R.; Kadakia, K.; Jampani, P.; Kumta, P. N. *Electrochim. Acta* **2011**, *56*, 4717–4723.
- (17) Wen, Z. S.; Lu, D.; Lei, J. P.; Fu, Y. Q.; Wang, L.; Sun, J. C. *J. Electrochem. Soc.* **2011**, *158*, A809–A813.
- (18) Zhou, W. C.; Upreti, S.; Whittingham, M. S. *Electrochem. Commun.* **2011**, *13*, 158–161.
- (19) Gao, P. F.; Nuli, Y.; He, Y. S.; Wang, J. Z.; Minett, A. I.; Yang, J.; Chen, J. *Chem. Commun.* **2010**, *46*, 9149–9151.
- (20) Eom, J. Y.; Kwon, H. S. *ACS Appl. Mater. Interfaces* **2011**, *3*, 1015–1021.

- (21) Chen, P. C.; Xu, J.; Chen, H. T.; Zhou, C. W. *Nano Res.* **2011**, *4*, 290–296.
- (22) Gomez-Camer, J. L.; Morales, J.; Sanchez, L. J. *Mater. Chem.* **2011**, *21*, 811–818.
- (23) Novoseolov, K. S.; Geim, A. K.; Morozov, S. V.; Jiang, D.; Zhang, Y.; Dubonos, S. V.; Grigorieva, I. V.; Firsov, A. A. *Science* **2004**, *306*, 666–669.
- (24) Wang, H.; Yang, Y.; Liang, Y.; Robinson, J. T.; Li, Y.; Jackson, A.; Cui, Y.; Dai, H. *Nano Lett.* **2011**, *11*, 2644–2647.
- (25) Wang, X.-L.; Han, W.-Q. *ACS Appl. Mater. Interfaces* **2010**, *2*, 3709–3713.
- (26) Jia, H.; Gao, P.; Yang, J.; Wang, J.; Nuli, Y.; Yang, Z. *Adv. Energy Mater.* **2011**, *1*, 1036–1039.
- (27) Zou, Y. Q.; Wang, Y. *Nanoscale* **2011**, *3*, 2615–2620.
- (28) Lv, W.; Sun, F.; Tang, D. M.; Fang, H. T.; Liu, C.; Yang, Q. H.; Cheng, H. M. *J. Mater. Chem.* **2011**, *21*, 9014–9019.
- (29) Ding, S. J.; Luan, D. Y.; Boey, F. Y. C.; Chen, J. S.; Lou, X. W. *Chem. Commun.* **2011**, *47*, 7155–7157.
- (30) Wu, Z. S.; Ren, W. C.; Wen, L.; Gao, L. B.; Zhao, J. P.; Chen, Z. P.; Zhou, G. M.; Li, F.; Cheng, H. M. *ACS Nano* **2010**, *4*, 3187–3194.
- (31) Wang, J. Z.; Zhong, C.; Chou, S. L.; Liu, H. K. *Electrochem. Commun.* **2010**, *12*, 1467–1470.
- (32) Lee, J. K.; Smith, K. B.; Hayner, C. M.; Kung, H. H. *Chem. Commun.* **2010**, *46*, 2025–2027.
- (33) Chou, S. L.; Wang, J. Z.; Choucair, M.; Liu, H. K.; Stride, J. A.; Dou, S. X. *Electrochem. Commun.* **2010**, *12*, 303–306.
- (34) Xiang, H.; Zhang, K.; Ji, G.; Lee, J. Y.; Zou, C.; Chen, X.; Wu, J. *Carbon* **2011**, *49*, 1787–1796.
- (35) Tao, H.-C.; Fan, L.-Z.; Mei, Y.; Qu, X. *Electrochem. Commun.* **2011**, *13*, 1332–1335.
- (36) Yang, S.; Li, G.; Zhu, Q.; Pan, Q. *J. Mater. Chem.* **2012**, *22*, 3420–3425.
- (37) Zhou, X.; Yin, Y.-X.; Wan, L.-J.; Guo, Y.-G. *Chem. Commun.* **2012**, *48*, 2198–2200.
- (38) Luo, J.; Zhao, X.; Wu, J.; Jang, H. D.; Kung, H. H.; Huang, J. J. *Phys. Chem. Lett.* **2012**, *3*, 1824–1829.
- (39) Chen, J. S.; Wang, Z.; Dong, X. C.; Chen, P.; Lou, X. W. *Nanoscale* **2011**, *3*, 2158–2161.
- (40) Zhu, J.; He, J. *ACS Appl. Mater. Interfaces* **2012**, *4*, 1770–1776.
- (41) Yang, S.; Feng, X.; Ivanovici, S.; Müllen, K. *Angew. Chem., Int. Ed.* **2010**, *49*, 8408–8411.
- (42) Li, D.; Müller, M. B.; Gilje, S.; Kaner, R. B.; Wallace, G. G. *Nat. Nanotechnol.* **2008**, *3*, 101–105.
- (43) Paraknowitsch, J. P.; Zhang, J.; Su, D.; Thomas, A.; Antonietti, M. *Adv. Mater.* **2010**, *22*, 87–92.
- (44) Lee, J. S.; Wang, X.; Luo, H.; Dai, S. *Adv. Mater.* **2010**, *22*, 1004–1007.
- (45) Wang, X.; Dai, S. *Angew. Chem.* **2010**, *122*, 6814–6818.
- (46) Ma, Z.; Yu, J.; Dai, S. *Adv. Mater.* **2010**, *22*, 261–285.
- (47) Paraknowitsch, J. P.; Thomas, A.; Antonietti, M. *J. Mater. Chem.* **2010**, *20*, 6746–6758.
- (48) Zhao, L.; Hu, Y.-S.; Li, H.; Wang, Z.; Chen, L. *Adv. Mater.* **2011**, *23*, 1385–1388.
- (49) Hummers, W. S.; Offeman, R. E. *J. Am. Chem. Soc.* **1958**, *80*, 1339.
- (50) Liang, Y.; Wu, D.; Feng, X.; Müllen, K. *Adv. Mater.* **2009**, *21*, 1679–1683.
- (51) Ferrari, A. C.; Meyer, J. C.; Scardaci, V.; Casiraghi, C.; Lazzeri, M.; Mauri, F.; Piscanec, S.; Jiang, D.; Novoselov, K. S.; Roth, S.; Geim, A. K. *Phys. Rev. Lett.* **2006**, *97*, 187401.
- (52) Kaniyoor, A.; Ramaprabhu, S. *AIP Adv.* **2012**, *2*, 032183.
- (53) Sobon, G.; Sotor, J.; Jagiello, J.; Kozinski, R.; Zdrojek, M.; Holdynski, M.; Paletko, P.; Boguslawski, J.; Lipinska, L.; Abramski, K. *M. Opt. Express* **2012**, *20*, 19463–19473.
- (54) Kim, T.; Mo, Y. H.; Nahm, K. S.; Oh, S. M. *J. Power Sources* **2006**, *162*, 1275–1281.
- (55) Cui, L.-F.; Yang, Y.; Hsu, C.-M.; Cui, Y. *Nano Lett.* **2009**, *9*, 3370–3374.
- (56) Wang, G. X.; Shen, X. P.; Yao, J.; Park, J. *Carbon* **2009**, *8*, 2049–2053.
- (57) Liang, M. H.; Zhi, L. J. *J. Mater. Chem.* **2009**, *19*, 5871–5878.
- (58) Gao, P.; Fu, J.; Yang, J.; Lv, R.; Wang, J.; Nuli, Y.; Tang, X. *Phys. Chem. Chem. Phys.* **2009**, *11*, 11101–11105.